

Pressure-induced polymorphism and piezochromism in $\text{Mn}_2\text{FeSbO}_6$

Cite as: Appl. Phys. Lett. **114**, 162903 (2019); doi: [10.1063/1.5090649](https://doi.org/10.1063/1.5090649)

Submitted: 29 January 2019 · Accepted: 6 April 2019 ·

Published Online: 23 April 2019










View Online



Export Citation



CrossMark

Lei Liu,^{1,a)}  Hong X. Song,^{2,b)}  Xiaodong Li,³  Dongzhou Zhang,⁴  Roland Mathieu,⁵  Sergey Ivanov,^{5,6}  Henrik Skogby,⁷ and Peter Lazor^{1,a)} 

AFFILIATIONS

¹Department of Earth Sciences, Uppsala University, Uppsala 75236, Sweden

²National Key Laboratory of Shock Wave and Detonation Physics, Institute of Fluid Physics, CAEP, Mianyang, Sichuan 621900, People's Republic of China

³Beijing Synchrotron Radiation Facility, Institute of High Energy Physics, China Academy of Science, Beijing 100049, China

⁴Partnership for Extreme Crystallography, University of Hawaii at Manoa, Honolulu, Hawaii 96822, USA

⁵Department of Engineering Sciences, Uppsala University, Uppsala 75121, Sweden

⁶Department of Inorganic Materials, Karpov's Institute of Physical Chemistry, Vorontsovo Pole, Moscow 105046, Russia

⁷Department of Geosciences, Swedish Museum of Natural History, Stockholm 10405, Sweden

^{a)}Authors to whom correspondence should be addressed: lei.liu@geo.uu.se and peter.lazor@geo.uu.se.

^{b)}Present address: Department of Chemistry, New York University, New York, New York 10003, USA.

ABSTRACT

In the last decade, major efforts have been devoted to searching for polar magnets due to their vast potential applications in spintronic devices. However, the polar magnets are rare because of conflicting electronic configuration requirements of ferromagnetism and electric polarization. Double-perovskite oxides with a polar structure containing transition metal elements represent excellent candidates for the polar magnet design. Herein, the crystal structure evolution of $\text{Mn}_2\text{FeSbO}_6$ (MFSO) was investigated at pressures reaching ~ 50 GPa by *in situ* synchrotron X-ray diffraction (XRD), Raman scattering, and *ab initio* calculation techniques. The XRD results reveal ilmenite- to perovskite-type phase transition at around 35 GPa. An additional intermediate phase, observed in the range of 31–36 GPa by Raman spectroscopy, but not the XRD technique, is proposed to represent the polar LiNbO_3 phase. It is argued that this phase emerged due to the heating effect of the Raman-excitation laser. The LiNbO_3 -type MFSO compounds, displaying an intrinsic dipole ordering, represent a promising candidate for multiferroic materials. The detected phase transitions were found to be reversible although a significant hysteresis was noticeable between compression and decompression runs. Moreover, a pressure-induced piezochromism, signifying a bandgap change, was discovered by the direct visual observations and corroborated by *ab initio* calculations. The present study benefits an efficient high-pressure synthesis of polar magnetic double-perovskite oxides in the future.

Published under license by AIP Publishing. <https://doi.org/10.1063/1.5090649>

Polar magnets, which possess strong coupling between magnetization and electric polarization in a single phase, are of great interest because of their magnetoelectric properties and potential applications in spintronic devices and information storage.^{1–7} However, owing to the incompatible electronic configuration requirements for the spin and dipole ordering,^{6,8,9} polar magnets are rare. Recently, $A_2BB'O_6$ double-perovskite oxides have been considered as a good platform for designing polar magnets.¹⁰ On one hand, $A_2BB'O_6$ can crystallize in noncentrosymmetric polar structures [for example, LiNbO_3 [LN, space group (s.g.) $R3c$],^{10,11} Ni_3TeO_6 (s.g. $R3$),¹² and ordered ilmenite (s.g. $R3$)¹³ structures] to create large spontaneous polarization (P_s). On

the other hand, transition-metal cations can occupy both A and B/B' sites, inducing a proper magnetism and enhancing the magnetoelectric coupling. The $A_2BB'O_6$ polar magnets were generally synthesized at appropriate high-pressure and high-temperature conditions to avoid the thermodynamically favorable centrosymmetric structures [ilmenite (IL, s.g. $R\bar{3}$) and perovskite (Pv) structure (s.g. $Pnma$ and $P2_1/n$), for example].^{10–14} Consequently, comprehensive studies on the crystal structure evolution of $A_2BB'O_6$ compounds as a function of pressure is a prerequisite for the efficient synthesis of $A_2BB'O_6$ polar magnets in the future. However, studies focusing on this topic have been scarce to date.^{15–18}

$\text{Mn}_2\text{FeSbO}_6$ (MFSO), melanostibite, is an extremely rare IL-type mineral discovered at the Sjögruvan locality in Sweden. This ferrimagnetic ($T_c \sim 270$ K) IL-type MFSO, as well as the antiferromagnetic perovskite-type MFSO (Pv, s.g. $P2_1/n$), can be synthesized as quenched products from high-pressure and high-temperature conditions.^{19–21} Unfortunately, both the IL and the Pv structures are centrosymmetric, and thus there are no P_s and small P_s , respectively, arising from the specific magnetic structure (type II multiferroic material²²). Very recently, a large magnetoelectric coupling effect was discovered in IL-type MFSO.²³ Consequently, supposing that MFSO with the polar structure (e.g., LN structure) can be synthesized, a promising multiferroic material with considerable P_s and large magnetoelectric coupling is expected.

Previous studies indicate that the LN structure is usually a retrograde product of the high-pressure Pv phase during decompression with a tolerance factor t smaller than 0.85^{24,25} [$t = (r_A + r_O)/(\sqrt{2}(r_B + r_O))$, where r_A , r_B , and r_O are the ionic radii of A, B, and O ions]. For MFSO, which has a tolerance factor of 0.78 and exhibits a high-pressure and temperature polymorphism with the Pv structure,²⁰ a transformation into the LN phase upon decompression is expected to occur. In addition, two MFSO analogs, $\text{Mn}_2\text{FeNbO}_6$ and $\text{Mn}_2\text{FeTaO}_6$, displaying the polar LN structure and obeying the tolerance factor criterion, were synthesized when quenched from high pressures and high temperatures.^{10,26} Both compounds showed high values of P_s , 32 $\mu\text{C}/\text{cm}^2$ for $\text{Mn}_2\text{FeNbO}_6$ and 23 $\mu\text{C}/\text{cm}^2$ for $\text{Mn}_2\text{FeTaO}_6$. Despite the similarity, the LN-type MFSO has not been synthesized yet, due to the different electronic configurations of the B' cations (Nb^{5+} and Ta^{5+} are d^0 cations, while Sb^{5+} is the d^{10} cation).¹⁰

In the present study, the structural evolution of a natural MFSO sample (mineral melanostibite) from the collections of the Swedish Museum of Natural History (NRM#g28947) was *in situ* investigated up to ~ 50 GPa by the synchrotron X-ray diffraction (XRD) and Raman scattering techniques, in combination with *ab initio* calculations. While the XRD results reveal only a single pressure-induced IL-to-Pv phase transition, Raman measurements also detect an intermediate phase above 30 GPa at a modest temperature (~ 400 K). We consider this as the missing LN phase of the MFSO compounds. Upon decompression, the LN-phase survives at pressure as low as 9.46 GPa.

Possessing a polar structure and transition-metal cations, the LN-type MFSO represents potentially a promising multiferroic material with large P_s and a strong magnetoelectric effect. The current results can serve as a guiding way for the synthesis of polar magnetic double-perovskite oxides in the future.

In the present study, the crystal structure evolution of MFSO under pressure has been investigated by using the *in situ* XRD technique at room temperature (see [supplementary material](#) for experimental details). The XRD patterns of MFSO collected upon compression are presented in Fig. 1. They reveal that the IL-type MFSO transforms to another structure at high pressures, as featured by two extra peaks growing [red and blue arrows in Fig. 1(c)] and one peak disappearing [dashed line in Fig. 1(c)]. The phase transition commenced at 34.74 GPa and was completed at 39.65 GPa. The XRD patterns of the high-pressure phase can be well reproduced using the structural model of synthetic Pv-type MFSO (Ref. 11, $P2_1/n$, see Fig. S1). This phase is stable up to 48.75 GPa. Upon decompression, it starts transforming back to the IL structure at 19.50 GPa although the Pv phase survives at pressures as low as 11.44 GPa (Fig. S2). No LN phase was detected during these quasi-hydrostatic compression and decompression runs, in contrast to what was observed with other Pv-type materials displaying small tolerance factors.²⁴ The significant hysteresis of the transition pressure indicates that a considerable kinetic barrier exists during this phase transition, involving the rearrangement of cations and bond breaking (Fig. S3 shows the details of the structural relationship between the IL and Pv structures). The pressure dependent volume data are fitted to the Vinet equation of state (EOS)²⁷

$$P = 3K_0 \left(\frac{V}{V_0} \right)^{-\frac{2}{3}} \left[1 - \left(\frac{V}{V_0} \right)^{-\frac{1}{3}} \right] \exp \left\{ \frac{3}{2} (K'_0 - 1) \left[1 - \left(\frac{V}{V_0} \right)^{-\frac{1}{3}} \right] \right\},$$

where V_0 is the equilibrium volume and K_0 and K'_0 are the bulk modulus and its pressure derivative at ambient pressure, respectively. The fits yield an equilibrium volume of $V_0 = 56.5(1) \text{ \AA}^3$ and a bulk modulus of $K_0 = 211(4) \text{ GPa}$ with K'_0 being fixed at 4 for the IL phase at ambient pressure (Fig. S4). This equilibrium volume agrees well with that of the synthetic MFSO with an IL structure (56.8 \AA^3).²⁰ For the Pv phase, the fit yields the bulk modulus of $K_0 = 229(4) \text{ GPa}$ when the

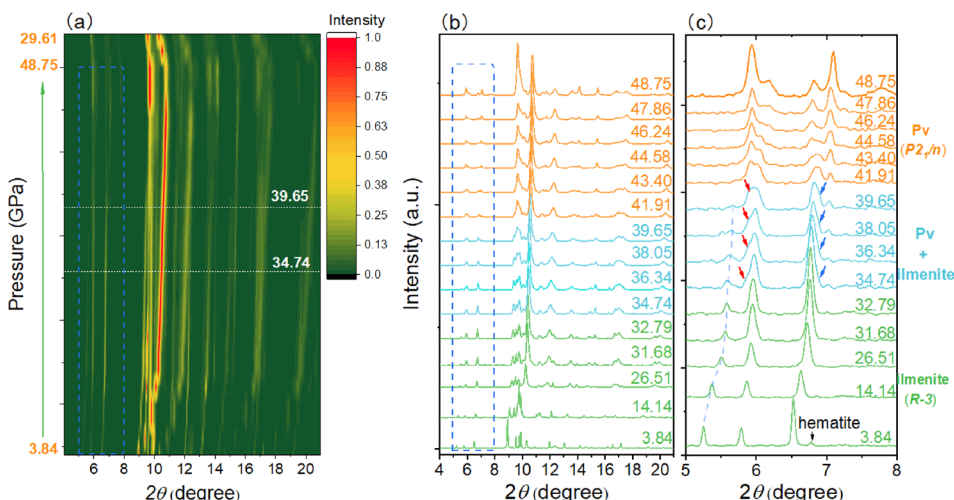


FIG. 1. High-pressure, room temperature XRD patterns of the powered MFSO. (a) Contour plot of 2D XRD patterns during compression from 3.84 GPa to 48.75 GPa and then decompression to 29.61 GPa. The intensity is normalized by its maximum value. (b) 1D XRD patterns as a function of pressure upon compression. The spectra are labeled with pressure values in gigapascal. (c) 1D XRD patterns in the range of 5° – 8° , according to the 2θ range indicated by the dashed blue boxes in (a) and (b). The dashed line indicates a peak disappearing, and the red and blue arrows indicate two extra peaks growing as pressure increases.

equilibrium volume V_0 is fixed at 54.1 \AA^3 , the value of the synthetic Pv phase²⁰ (Fig. S4). The volume collapse across the transition amounts to 2.6% at ~ 40 GPa.

Different from the XRD results, two phase transitions can readily be identified at 30.78 GPa and 36.15 GPa, when applying the technique of Raman spectroscopy on the single crystal of MFSO. The crystal was gradually compressed to 49.78 GPa while immersed in silicone oil (SO), which served as a pressure transmitting medium (PTM) [Figs. 2(a) and 2(b)]. These phase transitions recurred upon decompression at 32.29 GPa and 9.46 GPa [Figs. 2(c) and 2(d)].

Why did the phase transition pathways change when two different techniques, XRD and Raman spectroscopy, were employed? Generally, phase transitions of materials at high pressure can be affected by the forms of materials²⁸ (e.g., single crystal vs powder) and the stress environment in the sample chamber²⁹ (varying significantly when different PTMs are used). To probe these effects, two diamond anvil cells (DACs) loaded with the powdered MFSO sample and argon PTM were prepared. In each DAC, the sample was XRD-probed in the compression stage and Raman-probed upon decompression. Only one phase transition—IL to Pv—was observed by the XRD technique up to around 48 GPa, while two transitions were discovered during the decompression by the Raman technique (Figs. 2 and S5). Thus, both the powder sample using argon as PTM and the single crystal sample using SO PTM underwent two phase transitions at high pressures in the course of Raman measurements. This result indicates that the sample form and the stress environment are not the reasons accounting for the different phase transition routes found by the XRD and Raman scattering techniques.

One of the differences between the XRD and Raman techniques, which may play a role in the context of the current study, is that the

Raman excitation laser may cause local heating of the sample. The degree of laser absorption by a sample is largely controlled by the relationship between photons' energy and the sample's bandgap. In the present experiments, a laser power of 15–20 mW ($\lambda = 532$ nm and photon energy 2.33 eV) was focused to a spot size of 2–4 μm (see [supplementary material](#) for details). The energy gap of MFSO can be evaluated from the measured UV-vis absorption spectrum (Fig. S6). The deduced energy gaps at ambient pressure are 2.04 eV for the direct bandgap and 1.85 eV for the indirect bandgap. Both the values are smaller than the excitation laser photon energy of 2.33 eV. As pressure increases, the crystal color darkens (Fig. 3), which indicates a progressively narrower energy gap and an incremental increase in absorption of the laser power. This trend is confirmed by *ab initio* calculations (Fig. S7), which show that the rate of gap closure is meaningful on the applied experimental pressure scale. Thus, the heating effect due to laser absorption is not negligible in the course of Raman measurements, especially at high pressures. The local temperature of the probed sample spot was estimated using the intensity ratio of the corresponding Stokes and anti-Stokes Raman bands (see [supplementary material](#) for details). The temperature was found to increase up to around 400 K at 30.78 GPa where the first phase transition occurred (Fig. S7). Consequently, the heating effect of the excitation laser is implicated to represent the dominant factor behind the dissimilar phase transition routes observed by the XRD and Raman techniques. As we will discuss further on, the first phase transition represents a diffusion-type phase transition involving the rearrangement of cations and bond breaking. Elevated temperatures thus promote overcoming the high kinetic barrier.²⁰

What are the structures of the phases observed by Raman spectroscopy? Obviously, the starting phase has the IL structure. Its Raman

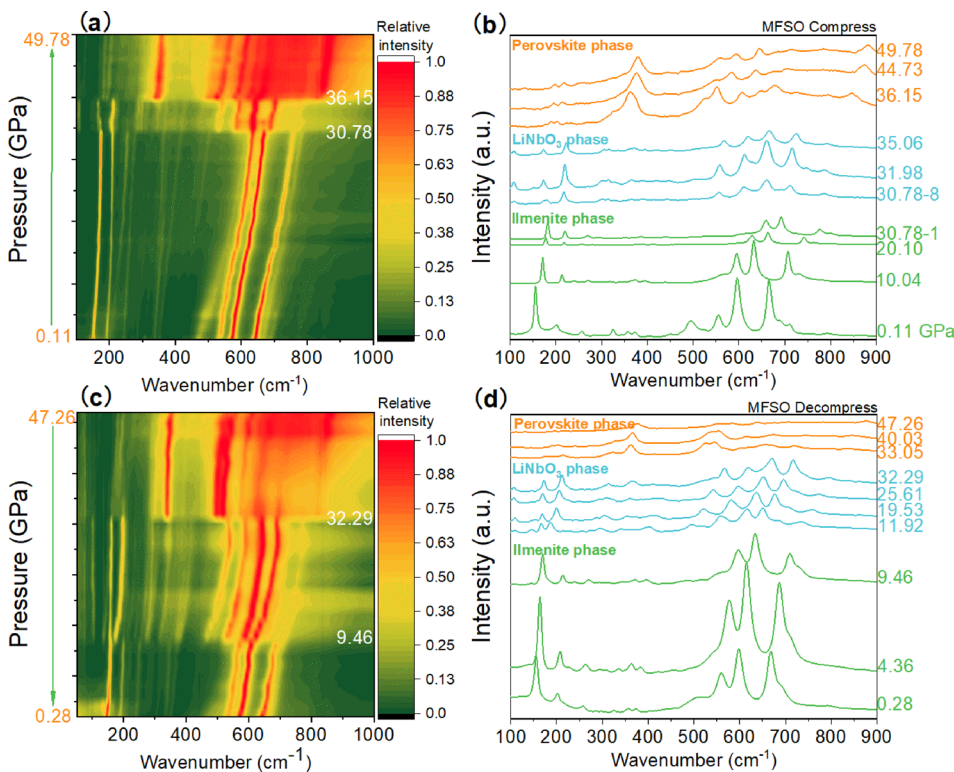


FIG. 2. Raman spectra of single crystal MFSO as a function of pressure. (a) Contour plot of 2D Raman spectra data during compression from 0.11 GPa to 49.78 GPa. (b) 1D Raman spectra as a function of pressure during compression. (c) Contour plot of 2D Raman spectra during decompression from 47.26 GPa to 0.28 GPa. (d) 1D Raman spectra as a function of pressure during decompression.

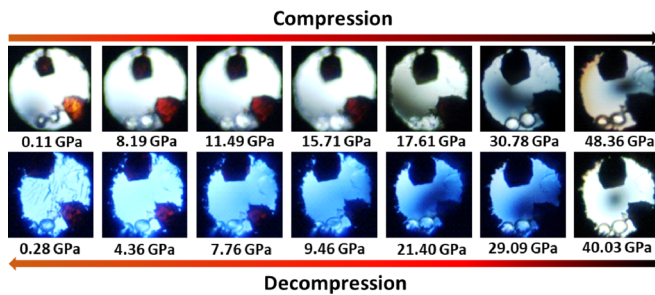


FIG. 3. Piezochromism of the MFSO crystal at high pressures upon compression and decompression. Pictures were taken in the transmission mode using white light. The crystal located in the upper part of the sample chamber appears darker owing to its larger thickness.

spectrum is consistent with that of the synthetic MFSO of the IL structure (Fig. S8).²³ All the 10 expected Raman active modes ($\Gamma = 5A_g + 5E_g$, s.g. $R\bar{3}$) have been determined and assigned. A few extra bands from the hematite (Fe_2O_3) impurity and the SO PTM are also present. According to the XRD results, the phase that appears at pressures above 36.75 GPa has the Pv structure (s.g. $P2_1/n$, Figs. 1 and S9). As for the intermediate phase appearing in the pressure range of 30.78–36.75 GPa upon compression, we argue that MFSO adopts the LN structure for the following two reasons:

- (1) Raman spectra support the LN structure. The calculated Raman modes of the LN-type MFSO agree fairly well with the experimental results at around 35 GPa, especially in the ranges of 150–300 cm^{-1} and 500–900 cm^{-1} (Fig. 4). Moreover, the Raman spectra of MFSO at around 35 GPa are similar to those of LN-type ZnTiO_3 ($R3c$) at high pressures as shown in Fig. 4.³⁰ For the LN-type materials, there are 13 Raman active modes ($\Gamma = 4A_1 + 9E$). 9 of the main peaks of LN-type ZnTiO_3 have the corresponding peaks in the Raman spectra of MFSO at around 35 GPa. The dashed blue lines in Fig. 4 indicate these peaks. The remaining bands of ZnTiO_3 originate from its minor Pv phase, and the extra bands of MFSO arise from the Raman modes not shown in ZnTiO_3 , as well as from the impurity, the intrinsic defects, and the LO-TO splitting.³¹ This similarity between the Raman spectra of MFSO and ZnTiO_3 with the LN structure indicates that both the compounds adopt the same symmetry at the corresponding conditions. Finally, the evolution of the Raman spectra from the LN phase to the Pv phase of ZnTiO_3 is similar to that observed during the second phase transition of MFSO at 36.75 GPa (Fig. S9). Consequently, we suggest that the observed intermediate phase is of the LN structure, while the high-pressure phase above 36.5 GPa has the Pv structure, as determined by the XRD technique.
- (2) The Goldschmidt diagram suggests that the LN-type quenched phase occurs for perovskite oxides with tolerance factors less than 0.85.²⁴ In this condition, the LN phase is usually a retrograde product of the high-pressure Pv phase during decompression.³² Two analogs of MFSO ($t = 0.78$), $\text{Mn}_2\text{FeNbO}_6$ and $\text{Mn}_2\text{FeTaO}_6$ with the polar LN structure, were synthesized as products quenched from high pressures and temperatures to ambient conditions.¹⁰ Because of the similar tolerance factor (the cation radii are 0.60 Å for Sb^{5+} and 0.64 Å for Nb^{5+} and Ta^{5+} when the coordination number is 6), the LN phase MFSO is also likely to appear. However, Li *et al.* did not obtain any LN phase MFSO from the quenched product.¹⁰ They argued that, in the case of tantalate and niobate, the second order Jahn–Teller (SOJT) distortion of the d^0 cations (Nb^{5+} and

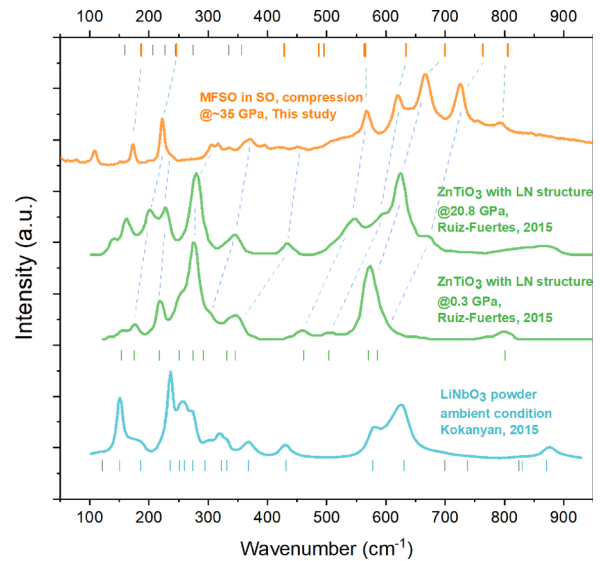


FIG. 4. Comparison of the Raman spectra of MFSO (crystal upon compression at 35 GPa), LiNbO_3 (powder at ambient conditions),³¹ and LN-type ZnTiO_3 (includes the minor Pv phase) at high pressures.³⁰ The tick marks at the bottom represent the Raman peak positions of LiNbO_3 powder (blue), including the extra bands (gray) originating from the intrinsic defects. The tick marks on the top represent the calculated Raman peak positions of LN-type MFSO. The gray ticks indicate the Raman modes with the intensity smaller than 1.5% of the strongest Raman mode.

Ta^{5+}) significantly lowered the energy and stabilized the LN over the IL structure.¹⁰ However, the LN-type ZnSnO_3 containing only d^{10} ions (Zn^{2+} and Sn^{4+}) without SOJT d^0 cations was synthesized, indicating that the presence of the SOJT d^0 ions is not necessary, and the polarity arising from the LN structure itself can stabilize this structure when using high-pressure and temperature synthesis.³³ Consequently, we consider that the LN phase MFSO can also be synthesized at high pressure and high temperature. The question arises whether this phase would be quenchable to room conditions. As shown by the Raman results, this is not the case, thus explaining why the LN structure has not been discovered in the products of previous high-pressure and high-temperature synthesis.^{10,20,23,34}

The phase diagram of MFSO is summarized in Fig. 5. The phase transition route of MFSO determined by Raman spectroscopy is IL-LN-Pv, different from the route IL-Pv observed by the XRD technique. The difference is ascribed to the heating effect of the Raman excitation laser. All the observed transitions have been found to be reversible although significant hysteresis exists between the compression and decompression runs. The LN phase is metastable with respect to the thermodynamically favored IL and Pv phases. We speculate that the LN phase, which has the potential to represent a promising multiferoic material, could be quenched to ambient pressure if an appropriately low-temperature decompression is applied.

In contrast to the previous synthesis experiments,^{20,23,34} the Pv phase has not been obtained upon decompression to ambient conditions in the current study. The present and previous results indicate that the Pv phase of MFSO is thermodynamically metastable but kinetically stable at room conditions. This metastable Pv phase is quenchable to room conditions, but the quenching process is highly dependent on the pressure-temperature loading routes and/or loading

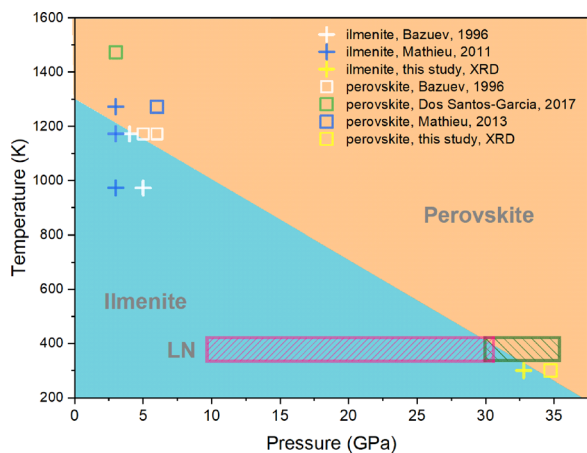


FIG. 5. Phase diagram of MFSO. The green shaded area represents the PT region of the metastable LN phase upon compression, and the pink shaded area represents the PT region of the metastable LN phase upon decompression, as determined in the course of Raman experiment.

rates, which we believe is the reason why the Pv phase of MFSO is not recovered in our experiments.

The crystal structural evolution of MFSO was investigated at pressures up to ~ 50 GPa using techniques of Raman spectroscopy and synchrotron x-ray diffraction. The transformation between two thermodynamically stable phases belonging to IL and Pv structures was observed at 35 GPa. Moreover, an intermediate metastable phase was also detected by the Raman scattering technique in the pressure range of 30.78–36.15 GPa, at around 400 K, and retained at a pressure as low as 9.46 GPa. This intermediate phase is proposed to be the missing polar LN structure of MFSO. We consider it potentially quenchable even down to ambient pressure if the synthesis conditions are carefully designed. The present results demonstrate that systematic studies on the phase transitions of $A_2BB'O_6$ compounds at high pressures and high temperatures are beneficial for guiding the synthesis of $A_2BB'O_6$ polar magnets.

See [supplementary material](#) for experimental details, refinement of crystal structures, evaluations of local temperature and bandgap energy, and Raman results from different runs.

This research was supported by Uppsala University. The XRD experiments were performed at GSECARS (Sector 13), Advanced Photon Source (APS). GSECARS is supported by the National Science Foundation-Earth Sciences (EAR-1634415) and Department of Energy-GeoSciences (DE-FG02-94ER14466). The PX2 program is supported by COMPRES under NSF Cooperative Agreement No. EAR-1661511. Parts of studies were performed at the 4W2 high-pressure station of BSRF, which is supported by the Chinese Academy of Sciences (Grant Nos. 11474281, KJCX2-SWN03, and KJCX2-SW-N20). We thank Professor Ulf Hålenius for the useful comments on the absorption spectrum of MFSO.

REFERENCES

- ¹W. Eerenstein, N. D. Mathur, and J. F. Scott, *Nature* **442**, 759 (2006).
- ²Y.-H. Chu, L. W. Martin, M. B. Holcomb, M. Gajek, S.-J. Han, Q. He, N. Balke, C.-H. Yang, D. Lee, W. Hu, Q. Zhan, P.-L. Yang, A. Fraile-Rodriguez, A. Scholl, S. X. Wang, and R. Ramesh, *Nat. Mater.* **7**, 478 (2008).

- ³W. Kleemann and P. Borisov, in *Smart Materials for Energy, Communications and Security*, edited by I. A. Lukýanchuk and D. Mezzane (Springer, The Netherlands, 2008), pp. 3–11.
- ⁴N. A. Spaldin, S.-W. Cheong, and R. Ramesh, *Phys. Today* **63**(10), 38 (2010).
- ⁵S. Dong, J.-M. Liu, S.-W. Cheong, and Z. Ren, *Adv. Phys.* **64**, 519 (2015).
- ⁶G.-H. Cai, M. Greenblatt, and M.-R. Li, *Chem. Mater.* **29**, 5447 (2017).
- ⁷N. Leo, V. Carolus, J. S. White, M. Kenzelmann, M. Hudl, T. Toledano, T. Honda, T. Kimura, S. A. Ivanov, M. Weil, Th. Lot-termoser, D. Meier, and M. Fiebig, *Nature* **560**, 466 (2018).
- ⁸N. A. Hill, *J. Phys. Chem. B* **104**, 6694 (2000).
- ⁹N. A. Benedek and C. J. Fennie, *J. Phys. Chem. C* **117**, 13339 (2013).
- ¹⁰M.-R. Li, D. Walker, M. Retuerto, T. Sarkar, J. Hadermann, P. W. Stephens, M. Croft, A. Ignatov, C. P. Grams, J. Hemberger, I. Nowik, P. S. Halasyamani, T. T. Tran, S. Mukherjee, T. S. Dasgupta, and M. Greenblatt, *Angew. Chem. Int. Ed.* **52**, 8406 (2013).
- ¹¹M.-R. Li, P. W. Stephens, M. Retuerto, T. Sarkar, C. P. Grams, J. Hemberger, M. Croft, D. Walker, and M. Greenblatt, *J. Am. Chem. Soc.* **136**, 8508 (2014).
- ¹²S. A. Ivanov, R. Mathieu, P. Nordblad, R. Tellgren, C. Ritter, E. Politova, G. Kaleva, A. Mosunov, S. Stefanovich, and M. Weil, *Chem. Mater.* **25**, 935 (2013).
- ¹³M.-R. Li, M. Retuerto, P. W. Stephens, M. Croft, D. Sheptyakov, V. Pomjakushin, Z. Deng, H. Akamatsu, V. Gopalan, J. Sánchez-Benitez, F. O. Saouma, J. I. Jang, D. Walker, and M. Greenblatt, *Angew. Chem. Int. Ed.* **55**, 9862 (2016).
- ¹⁴E. Solana-Madruga, A. J. Dos Santos-Garcia, A. M. Arevalo-Lopez, D. Avila-Brandé, C. Ritter, J. P. Attfield, and R. Saer-Puche, *Dalton Trans.* **44**, 20441 (2015).
- ¹⁵J. S. Olsen, L. Gerward, G. Vaitheeswaran, V. Kanchana, and L. Alff, *High Pressure Res.* **29**, 83 (2009).
- ¹⁶B. Manoun, J. M. Igartua, M. Gateshki, and S. K. Saxena, *J. Mol. Struct.* **888**, 244 (2008).
- ¹⁷N. Li, B. Manoun, L. Tang, F. Ke, F. Liu, H. Dong, P. Lazor, and W. Yang, *Inorg. Chem.* **55**, 6770 (2016).
- ¹⁸E. Gilioli and L. Ehm, *IUCr* **1**, 590 (2014).
- ¹⁹R. Mathieu, S. A. Ivanov, I. V. Solovyev, G. V. Bazuev, M. Hudl, P. Lazor, I. V. Solovyev, and P. Nordblad, *Appl. Phys. Lett.* **98**, 202505 (2011).
- ²⁰R. Mathieu, S. A. Ivanov, I. V. Solovyev, G. V. Bazuev, P. A. Kumar, P. Lazor, and P. Nordblad, *Phys. Rev. B* **87**, 014408 (2013).
- ²¹M. Hudl, R. Mathieu, P. Nordblad, S. A. Ivanov, G. V. Bazuev, and P. Lazor, *J. Magn. Magn. Mater.* **331**, 193 (2013).
- ²²D. Khomskii, *Physics* **2**, 20 (2009).
- ²³A. J. Dos Santos-Garcia, E. Solana-Madruga, C. Ritter, A. Andra-da-Chacon, J. Sanchez-Benitez, F. J. Mompean, M. Garcia-Hernandez, R. Saez-Puche, and R. Schmidt, *Angew. Chem. Int. Ed.* **56**, 4438 (2017).
- ²⁴H. Yusa, “Structural relaxation of oxide compounds from the high-pressure phase,” in *Nanoinformatics*, edited by I. Tanaka (Springer, Singapore, 2017), pp. 259–278.
- ²⁵C. T. Prewitt, T. Ko, G. Shen, and J. D. F. Gerald, *Rev. High Pressure Sci. Technol.* **7**, 40 (1998).
- ²⁶A. J. Dos Santos-Garcia, E. Solana-Madruga, C. Ritter, D. Avila-Brandé, O. Fabelo, and R. Saez-Puche, *Dalton Trans.* **44**, 10665 (2015).
- ²⁷P. Vinet, J. Ferrante, J. H. Rose, and J. R. Smith, *J. Geophys. Res.* **92**, 9319, <https://doi.org/10.1029/JB092iB09p09319> (1987).
- ²⁸H. T. Girao, P. Hermet, B. Masenelli, J. Haines, P. Melinon, and D. Machon, *Phys. Rev. Lett.* **120**, 265702 (2018).
- ²⁹F. Yang, Y. Lin, J. E. P. Dahl, R. M. K. Carlson, and W. L. Mao, *J. Chem. Phys.* **141**, 154305 (2014).
- ³⁰J. Ruiz-Fuertes, B. Winkler, T. Bernert, L. Bayarjargal, W. Mor-genroth, M. Kock-Muller, K. Refson, V. Milman, and N. Tamura, *Phys. Rev. B* **91**, 214110 (2015).
- ³¹N. Kokanyan, *Study of Photo-Electrostrictive Effects in Photore-fractive LiNbO3 Probed by Polarized Raman Spectroscopy* (Université de Lorraine, Nancy, 2015).
- ³²A. Navrotsky, *Chem. Mater.* **10**, 2787 (1998).
- ³³Y. Inaguma, A. Aimi, Y. Shirako, D. Sakurai, D. Mori, H. Kojitani, M. Akaogi, and M. Nakayama, *J. Am. Chem. Soc.* **136**, 2748 (2014).
- ³⁴G. V. Bazuev, B. G. Golovkin, N. V. Lukin, N. I. Kadyrova, and Y. G. Zainulin, *J. Solid State Chem.* **124**, 333 (1996).